Supporting Information

Multifunctional Ln^{III} complexes constructed by selected phosphine oxide and diketonate in association with SMM, luminescent and MCE properties

Han Yan [a], Zi-Wei Che [a] and Wen-Bin Sun[a]*

a. *Key Laboratory of Functional Inorganic Material Chemistry Ministry of Education, School of Chemistry and Material Science Heilongjiang University, 74 Xuefu Road, Harbin 150080, P. R. China.*

E-mail: wenbinsun@126.com

Table S1. Crystallographic data for **1**-**3**.

	1	**2**	**3**
Empirical formula	$C_{51}H_{72}DyO_7P$	$C_{92}H_{138}Dy_2O_{14}P_2$	$C_{56}H_{70}Dy_2O_{16}P_2$
FW ($g.mol^{-1}$)	990.55	1854.96	1386.06
Crystal system	monoclinic	Triclinic	Triclinic
Space group	$P2_1/n$	P-1	P-1
Temperature (K)	298	298	293
a (Å)	15.1425(7)	13.1963(6)	11.0237(6)
b (Å)	19.2903(12)	13.9250(7)	12.2222(6)
c (Å)	19.2838(9)	15.1757(5)	12.2882(6)
α (°)	90	85.183(3)	166.833(5)
β (°)	95.401(4)	86.395(3)	94.721(4)
γ (°)	90	62.322(5)	90.589(6)
V ($Å^3$)	5607.9(5)	2459.9(2)	1470.28(14)
ρ_{cacd} ($Mg.m^{-3}$)	1.173	1.252	1.565
μ (mm^{-1})	1.403	1.594	2.641
F(000)	2060.0	964.0	696.0
Independent relections	9862	11255	6785
R_{int}	0.0461	0.0442	0.0278
R_1 [I > 2σ(I)]	0.0854	0.0487	0.0295
wR_2 (all data)	0.2807	0.0805	0.0614
Goodness of fit on F^2	1.056	0.923	1.038
CCDC numbers	2181171	2181172	2181173

Table S2. Crystallographic data for **4**-**6**.

	4	**5**	**6**
Empirical formula	$C_{56}H_{70}Gd_2O_{16}P_2$	$C_{56}H_{70}Eu_2O_{16}P_2$	$C_{56}H_{70}Tb_2O_{16}P_2$
FW ($g.mol^{-1}$)	1375.56	1364.98	1378.90
Crystal system	Triclinic	Triclinic	Triclinic
Space group	P-1	P-1	P-1
Temperature (K)	298	298	298
a (Å)	11.0947(6)	11.1109(7)	11.0522(5)
b (Å)	12.2688(7)	12.2670(8)	12.2463(4)
c (Å)	12.3032(7)	12.2742(9)	12.2833(5)
α (°)	116.703(6)	116.611(7)	116.775(4)
β (°)	94.714(4)	94.872(6)	94.703(3)
γ (°)	90.564(4)	90.557(5)	90.557(3)
V ($Å^3$)	1488.97(16)	1488.18(19)	1477.24(11)
ρ_{cacd} ($Mg.m^{-3}$)	1.534	1.523	1.550
μ (mm^{-1})	2.326	2.206	2.493
F(000)	692.0	690.0	694.0
Independent relections	5192	5236	6723
R_{int}	0.0685	0.0658	0.0300
R_1 [I > 2σ(I)]	0.0443	0.0535	0.0326
wR_2 (all data)	0.0544	0.1177	0.0591
Goodness of fit on F^2	0.907	0.961	0.978
CCDC numbers	2181174	2181175	2181176

Table S3. Selected bond lengths (Å) and angles (°) for **1**.

Dy1-O1	2.316(6)	Dy1-O6	2.307(7)
Dy1-O2	2.32(3)	Dy1-O7	2.255(7)
Dy1-O4	2.184(3)	Dy1-O5	2.21(2)
Dy1-O3	2.309(4)		
O2-Dy1-O1	140.2(9)	O6-Dy1-O3	147.3(3)
O4-Dy1-O1	88.2(6)	O7-Dy1-O1	83.4(3)
O4-Dy1-O2	109.5(14)	O7-Dy1-O2	79.9(13)
O4-Dy1-O3	82.9(5)	O7-Dy1-O3	99.3(2)
O4-Dy1-O6	87.4(6)	O7-Dy1-O6	85.8(3)
O4-Dy1-O7	170.5(6)	O5-Dy1-O1	146.9(15)
O4-Dy1-O5	74.0(17)	O5-Dy1-O2	72.8(17)
O3-Dy1-O1	75.7(4)	O5-Dy1-O3	127.5(17)
O3-Dy1-O2	71.8(4)	O5-Dy1-O6	78.6(16)
O6-Dy1-O1	72.8(3)	O5-Dy1-O7	111.1(17)
O6-Dy1-O2	140.6(4)		

Table S4. Selected bond lengths (Å) and angles (°) for **2**.

Dy1-O7	2.320(3)	Dy1-O2	2.308(3)
Dy1-O6	2.294(3)	Dy1-O4	2.302(3)
Dy1-O5	2.251(2)	Dy1-O3	2.272(3)
Dy1-O1	2.290(2)		
O6-Dy1-O7	72.55(9)	O1-Dy1-O2	78.28(9)
O6-Dy1-O2	79.10(9)	O1-Dy1-O4	79.84(9)
O6-Dy1-O4	146.14(10)	O2-Dy1-O7	130.51(10)
O5-Dy1-O7	85.32(10)	O4-Dy1-O7	81.40(10)
O5-Dy1-O6	81.40(9)	O4-Dy1-O2	134.76(10)
O5-Dy1-O1	151.48(9)	O3-Dy1-O7	156.66(10)
O5-Dy1-O2	129.61(10)	O3-Dy1-O6	123.78(11)
O5-Dy1-O4	75.17(9)	O3-Dy1-O1	106.03(11)
O5-Dy1-O3	81.45(11)	O3-Dy1-O2	72.13(10)
O1-Dy1-O7	77.51(9)	O3-Dy1-O4	76.68(11)
O1-Dy1-O6	114.04(10)		

Table S5. Selected bond lengths (Å) and angles (°) for **3**.

Dy1-O3	2.388(2)	Dy1-O4	2.306(2)
Dy1-O7	2.341(2)	Dy1-O2	2.424(2)
Dy1-O5	2.365(2)	Dy1-O6	2.317(2)
Dy1-O1	2.360(2)	Dy1-O8	2.338(2)
O3-Dy1-O2	73.63(7)	O4-Dy1-O2	141.93(7)
O7-Dy1-O3	136.71(8)	O4-Dy1-O6	73.73(8)
O7-Dy1-O5	75.67(8)	O4-Dy1-O8	85.74(8)
O7-Dy1-O1	112.45(8)	O6-Dy1-O3	119.95(8)
O7-Dy1-O2	69.26(7)	O6-Dy1-O7	79.39(8)
O5-Dy1-O3	74.89(8)	O6-Dy1-O5	72.42(8)
O5-Dy1-O2	76.88(7)	O6-Dy1-O1	140.30(8)
O1-Dy1-O3	78.34(8)	O6-Dy1-O2	140.48(8)
O1-Dy1-O5	146.18(7)	O6-Dy1-O8	76.13(8)
O1-Dy1-O2	76.02(7)	O8-Dy1-O3	146.41(8)
O4-Dy1-O3	72.81(7)	O8-Dy1-O7	71.82(8)
O4-Dy1-O7	148.42(7)	O8-Dy1-O5	138.06(7)
O4-Dy1-O5	110.66(8)	O8-Dy1-O1	72.61(7)
O4-Dy1-O1	80.08(8)	O8-Dy1-O2	114.10(8)

Table S6. Selected bond lengths (Å) and angles (°) for **4**.

Gd1-O3	2.373(3)	Gd1-O2	2.447(2)
Gd1-O1	2.386(3)	Gd1-O5	2.348(3)
Gd1-O6	2.395(3)	Gd1-O4	2.371(3)
Gd1-O7	2.423(3)	Gd1-O8	2.334(3)
O3-Gd1-O1	72.67(11)	O5-Gd1-O2	139.92(10)
O3-Gd1-O6	137.60(12)	O5-Gd1-O4	79.26(12)
O3-Gd1-O7	146.63(11)	O4-Gd1-O3	71.29(12)
O3-Gd1-O2	114.31(11)	O4-Gd1-O1	112.01(11)
O1-Gd1-O6	146.51(10)	O4-Gd1-O6	75.90(12)
O1-Gd1-O7	78.69(11)	O4-Gd1-O7	137.21(11)
O1-Gd1-O2	76.39(9)	O4-Gd1-O2	69.19(10)
O6-Gd1-O7	75.05(11)	O8-Gd1-O3	86.18(12)
O6-Gd1-O2	76.66(10)	O8-Gd1-O1	80.14(11)
O7-Gd1-O2	73.99(10)	O8-Gd1-O6	110.51(12)
O5-Gd1-O3	76.02(12)	O8-Gd1-O7	72.17(11)
O5-Gd1-O1	140.42(10)	O8-Gd1-O2	141.83(10)
O5-Gd1-O6	72.07(11)	O8-Gd1-O5	74.16(12)
O5-Gd1-O7	119.70(12)	O8-Gd1-O4	148.61(11)

Table S7. Selected bond lengths (Å) and angles (°) for **5**.

Eu1-O2	2.465(5)	Eu1-O8	2.366(5)
Eu1-O3	2.427(5)	Eu1-O1	2.401(5)
Eu1-O6	2.403(5)	Eu1-O5	2.360(5)
Eu1-O7	2.374(5)	Eu1-O4	2.338(5)
O3-Eu1-O2	73.94(16)	O1-Eu1-O6	146.83(16)
O6-Eu1-O2	76.65(17)	O5-Eu1-O2	139.59(16)
O6-Eu1-O3	75.28(16)	O5-Eu1-O3	119.45(19)
O7-Eu1-O2	69.59(16)	O5-Eu1-O6	71.47(16)
O7-Eu1-O3	137.55(17)	O5-Eu1-O7	78.90(19)
O7-Eu1-O6	75.83(18)	O5-Eu1-O8	76.39(19)
O7-Eu1-O1	112.30(18)	O5-Eu1-O1	140.64(17)
O8-Eu1-O2	114.26(18)	O4-Eu1-O2	141.44(15)
O8-Eu1-O3	146.82(17)	O4-Eu1-O3	71.54(17)
O8-Eu1-O6	137.22(16)	O4-Eu1-O6	110.0(2)
O8-Eu1-O7	70.81(17)	O4-Eu1-O7	148.72(17)
O8-Eu1-O1	72.73(16)	O4-Eu1-O8	87.13(19)
O1-Eu1-O2	76.68(16)	O4-Eu1-O1	80.19(19)
O1-Eu1-O3	78.66(16)	O4-Eu1-O5	74.41(18)

Table S8. Selected bond lengths (Å) and angles (°) for **6**.

Tb1-O3	2.400(2)	Tb1-O6	2.379(2)
Tb1-O2	2.436(2)	Tb1-O1	2.369(2)
Tb1-O8	2.357(2)	Tb1-O5	2.328(2)
Tb1-O7	2.353(2)	Tb1-O4	2.315(2)
O3-Tb1-O2	73.66(8)	O1-Tb1-O6	146.39(7)
O8-Tb1-O3	136.98(8)	O5-Tb1-O3	119.96(9)
O8-Tb1-O2	69.30(7)	O5-Tb1-O2	140.23(7)
O8-Tb1-O6	75.73(8)	O5-Tb1-O8	79.33(8)
O8-Tb1-O1	112.13(8)	O5-Tb1-O7	76.13(8)
O7-Tb1-O3	146.46(8)	O5-Tb1-O6	72.20(8)
O7-Tb1-O2	114.18(8)	O5-Tb1-O1	140.39(8)
O7-Tb1-O8	71.46(8)	O4-Tb1-O3	72.66(8)
O7-Tb1-O6	137.74(7)	O4-Tb1-O2	141.97(7)
O7-Tb1-O1	72.60(8)	O4-Tb1-O8	148.36(8)
O6-Tb1-O3	75.17(7)	O4-Tb1-O7	85.96(9)
O6-Tb1-O2	76.75(8)	O4-Tb1-O6	110.63(9)
O1-Tb1-O3	78.42(8)	O4-Tb1-O1	80.27(8)
O1-Tb1-O2	76.15(7)	O4-Tb1-O5	73.81(8)

Table S9. Continuous Shape Measures (CShMs) of the coordination geometry in compounds **1**-**6**. The three closer ideal geometries to the real complexes are listed and below are the symmetry and description for each polyhedron.

Complex		*s*	Polyhedron		
1	Dy1	1.645	CTPR-7	C2v	Capped trigonal prism
		2.082	COC-7	C3v	Capped octahedron
		2.990	PBPY-7	D5h	Pentagonal bipyramid
2	Dy1	0.467	COC-7	C3v	Capped octahedron
		1.074	CTPR-7	C2v	Capped trigonal prism
		6.639	PBPY-7	D5h	Pentagonal bipyramid
	Dy1’	0.467	COC-7	C3v	Capped octahedron
		1.074	CTPR-7	C2v	Capped trigonal prism
		6.639	PBPY-7	D5h	Pentagonal bipyramid
3	Dy1	0.373	SAPR-8	D4d	Square antiprism
		1.988	BTPR-8	C2v	Biaugmented trigonal prism
		2.011	TDD-8	D2d	Triangular dodecahedron
	Dy1’	0.373	SAPR-8	D4d	Square antiprism
		1.988	BTPR-8	C2v	Biaugmented trigonal prism
		2.011	TDD-8	D2d	Triangular dodecahedron
4	Gd1	0.394	SAPR-8	D4d	Square antiprism
		2.016	BTPR-8	C2v	Biaugmented trigonal prism
		2.074	TDD-8	D2d	Triangular dodecahedron
	Gd1’	0.394	SAPR-8	D4d	Square antiprism
		2.016	BTPR-8	C2v	Biaugmented trigonal prism
		2.074	TDD-8	D2d	Triangular dodecahedron
5	Eu1	0.429	SAPR-8	D4d	Square antiprism
		1.994	BTPR-8	C2v	Biaugmented trigonal prism
		2.049	TDD-8	D2d	Triangular dodecahedron
	Eu1’	0.429	SAPR-8	D4d	Square antiprism
		1.994	BTPR-8	C2v	Biaugmented trigonal prism
		2.049	TDD-8	D2d	Triangular dodecahedron
6	Tb1	0.383	SAPR-8	D4d	Square antiprism
		1.997	BTPR-8	C2v	Biaugmented trigonal prism
		2.047	TDD-8	D2d	Triangular dodecahedron
	Tb1’	0.383	SAPR-8	D4d	Square antiprism
		1.997	BTPR-8	C2v	Biaugmented trigonal prism
		2.047	TDD-8	D2d	Triangular dodecahedron

Table S10. Best fitted parameters (χ_T, χ_S, τ and α) with the extended Debye model for complex **1** at 800 Oe in the temperature range 2-4.5 K.

T/ K	χ_S / cm^3 mol^{-1}	χ_T / cm^3 mol^{-1}	τ/s	α
2	0.32902	5.98389	0.00626	0.26029
2.5	0.35777	4.78013	0.00314	0.18052
3	0.33282	4.06174	0.00158	0.13437
3.5	0.32543	3.50318	0.00079	0.09153
4	0.33101	3.08828	0.00041	0.06547
4.5	0.37385	2.76536	0.00023	0.04999

Table S11. Best fitted parameters (χ_T, χ_S, τ and α) with the extended Debye model for complex **2** at 1500 Oe in the temperature range 3-8.5 K.

T/ K	χ_S / cm^3 mol^{-1}	χ_T / cm^3 mol^{-1}	τ/s	α
3	0.14156	10.40643	0.13001	0.28921
3.5	0.19116	8.24229	0.04459	0.27579
4	0.30461	6.92120	0.01826	0.23698
4.5	0.45242	6.06284	0.00882	0.19054
5	0.54450	5.45665	0.00476	0.15468
5.5	0.56214	4.97633	0.00270	0.13373
6	0.54373	4.60324	0.00163	0.12911
6.5	0.52072	4.27870	0.00100	0.12909
7	0.52186	3.99742	0.00065	0.12759
7.5	0.54846	3.74438	0.00043	0.12398
8	0.61211	3.51809	0.00030	0.11722
8.5	0.91669	3.31669	0.00021	0.10963

Table S12. Best fitted parameters (χ_T, χ_S, τ and α) with the extended Debye model for complex **3** at 1500 Oe in the temperature range 3-8 K.

T/ K	χ_S / cm^3 mol^{-1}	χ_T / cm^3 mol^{-1}	τ/s	α
3	0.34672	8.50440	0.13255	0.13727
3.5	0.25665	7.24854	0.05122	0.13438
4	0.20806	6.34888	0.02015	0.12974
4.5	0.16965	5.72243	0.00850	0.11491
5	0.15203	5.17176	0.00399	0.09909
5.5	0.12936	4.76839	0.00205	0.09307
6	0.12056	4.35878	0.00111	0.07952
6.5	0.09583	4.08468	0.00066	0.08137
7	0.13116	3.78427	0.00041	0.06039
7.5	0.21562	3.53164	0.00027	0.03625
8	0.24302	3.33775	0.00018	0.03133

Table S13. Best fitted parameters (χ_T, χ_S, τ and α) with the extended Debye model for complex **3** at 0 Oe in the temperature range 2-7.5 K.

T/ K	χ_S / cm^3 mol^{-1}	χ_T / cm^3 mol^{-1}	τ/s	α
2	5.90646	0.11094	0.00069	0.19061
2.5	4.66657	8.95381	0.00063	0.19781
3	3.72740	7.49116	0.00056	0.21871
3.5	2.99131	6.40937	0.00049	0.22468
4	3.40803	5.58945	0.00073	0.12321
4.5	3.02332	4.96855	0.00067	0.11677
5	2.74901	4.46769	0.00062	0.09502
5.5	2.48808	4.05524	0.00052	0.07644
6	2.28395	3.72233	0.00043	0.05449
6.5	2.09396	3.44299	0.00033	0.04459
7	1.94474	3.19346	0.00025	0.02909

7.5	1.84069	2.98388	0.00019	0.00978

Table S14 The curves are fitted by the modified Arrhenius relationship the QTM process is taken account $1/\tau = 1/\tau_{QTM} + CT^n + \tau_0^{-1}\exp(-U_{eff}/\kappa T)$.

complex	τ_{QTM} (s)	C ($s^{-1}\cdot K^{-n}$)	n	τ_0 (s)	U_{eff}/κ_B (K)
3	6.25×10^{-4}	1.29×10^{2}	1.60	5.13×10^{-6}	27.12

Table S15 The curves are fitted by the modified Arrhenius relationship the Raman process is taken account $1/\tau = CT^n + \tau_0^{-1}\exp(-U_{eff}/\kappa T)$.

complex	C ($s^{-1}\cdot K^{-n}$)	n	τ_0 (s)	U_{eff}/κ_B (K)
1	1.05×10^{1}	3.39	3.46×10^{-6}	19.03
2	1.39×10^{-2}	6.03	1.03×10^{-6}	44.87
3	5.62×10^{-3}	6.54	6.42×10^{-7}	45.22

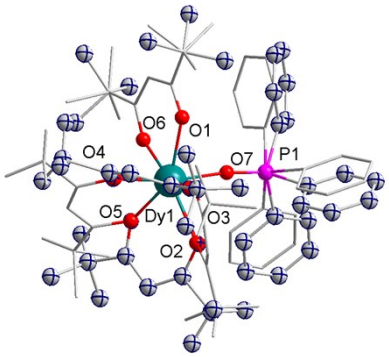

Fig. S1 Partially labeled molecular structure of complexes **1**, the part of the disorder is shown as front ellipse in blue line. Color code: Dy (teal), P (pink), O (red), C (grey).

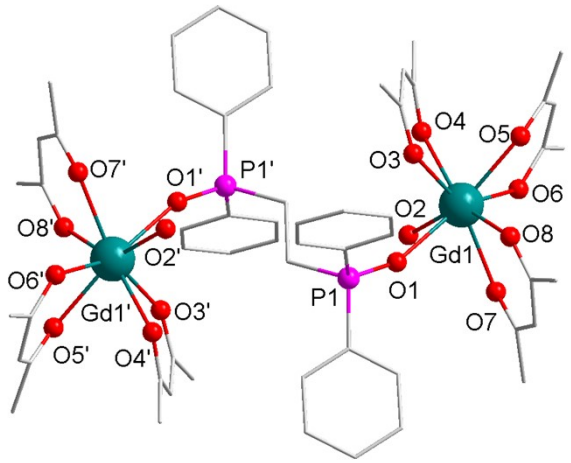

Fig. S2 Partially labeled molecular structure of complexes **4**. Color code: Gd (teal), P (pink), O (red), C (grey).

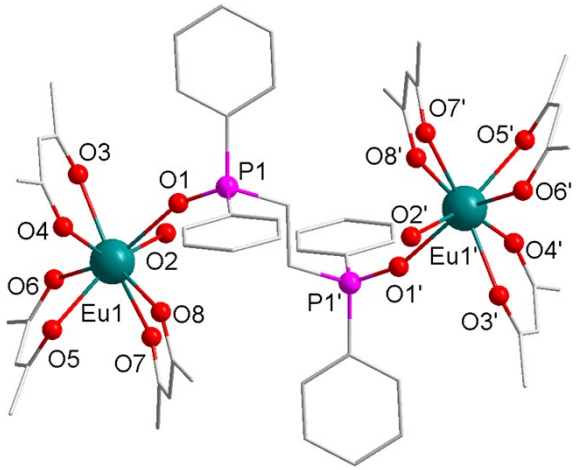

Fig. S3 Partially labeled molecular structure of complexes **5**. Color code: Eu (teal), P (pink), O (red), C (grey).

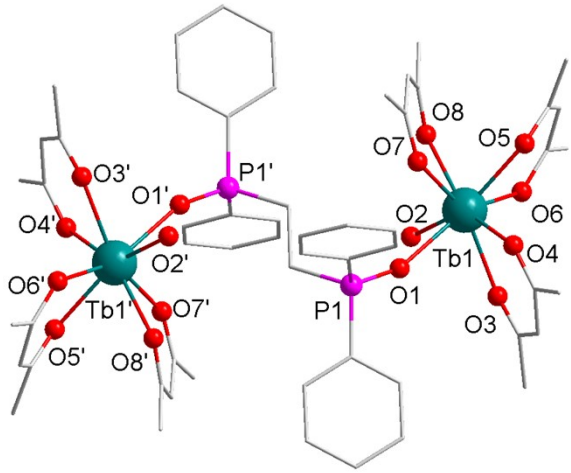

Fig. S4 Partially labeled molecular structure of complexes **6**. Color code: Tb (teal), P (pink), O (red), C (grey).

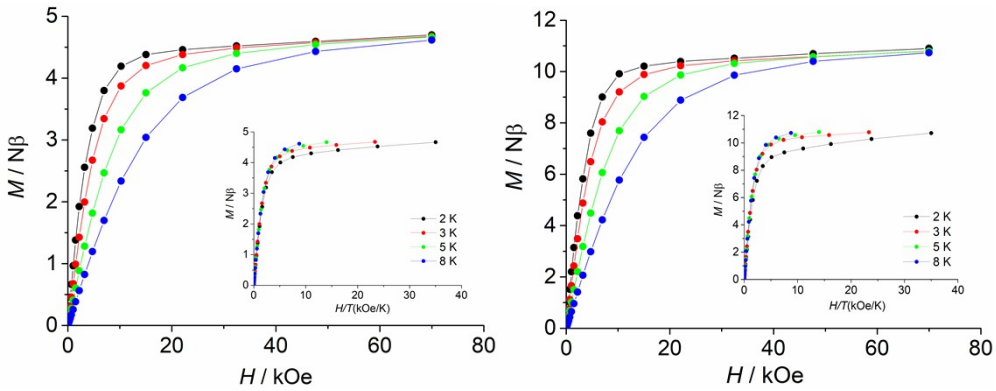

Fig. S5 Field dependence of the magnetization between 2 and 8 K for **1** and **2**.

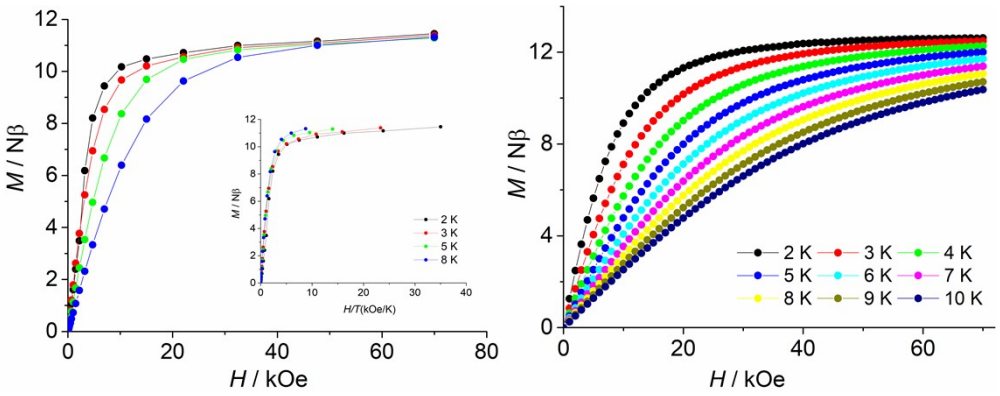

Fig. S6 Field dependence of the magnetization between 2 and 8 K for **3** and **4**.

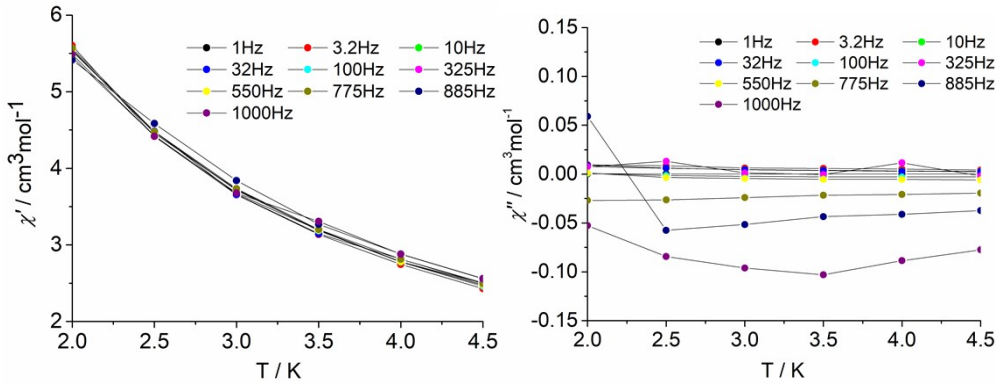

Fig. S7 The temperature dependent in-phase (χ') and out-of-phase (χ'') ac susceptibility under 0 Oe field for **1.**

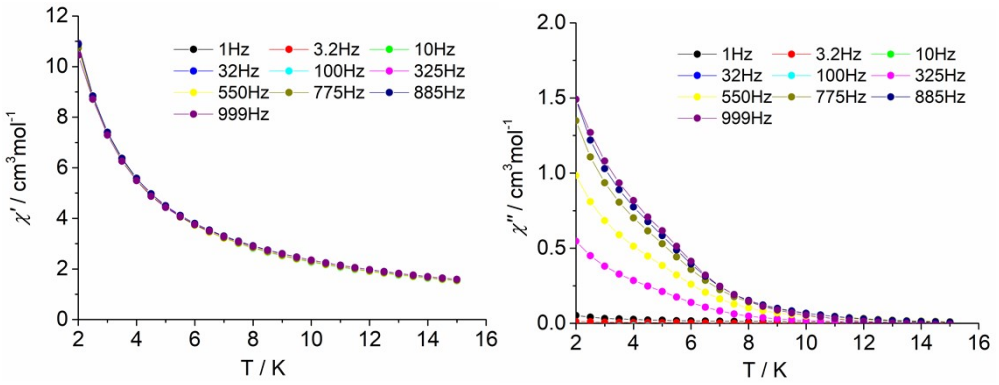

Fig. S8 The temperature dependent in-phase (χ') and out-of-phase (χ'') ac susceptibility under 0 Oe field for **2.**

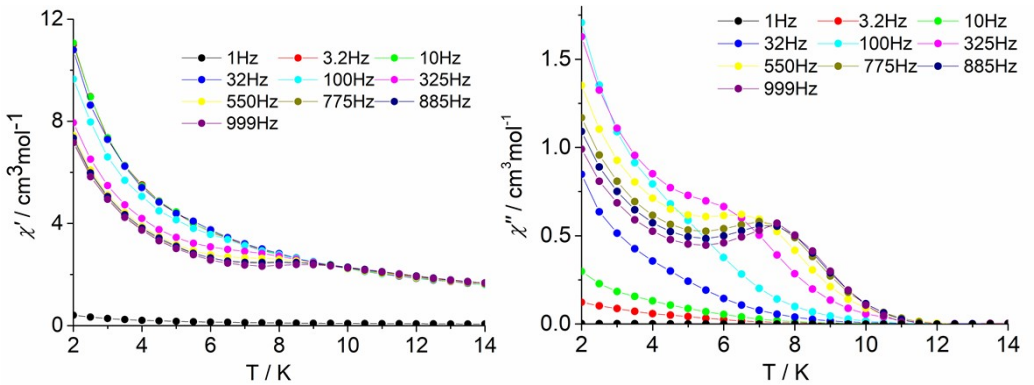

Fig. S9 The temperature dependent in-phase (χ') and out-of-phase (χ'') ac susceptibility under 0 Oe field for **3**.

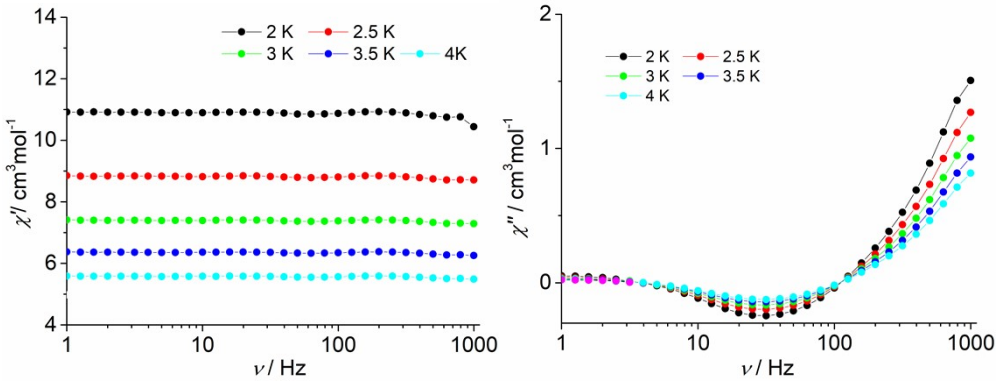

Fig. S10 The frequency dependent in-phase (χ') and out-of-phase (χ'') ac susceptibility under 0 Oe field for **2.**

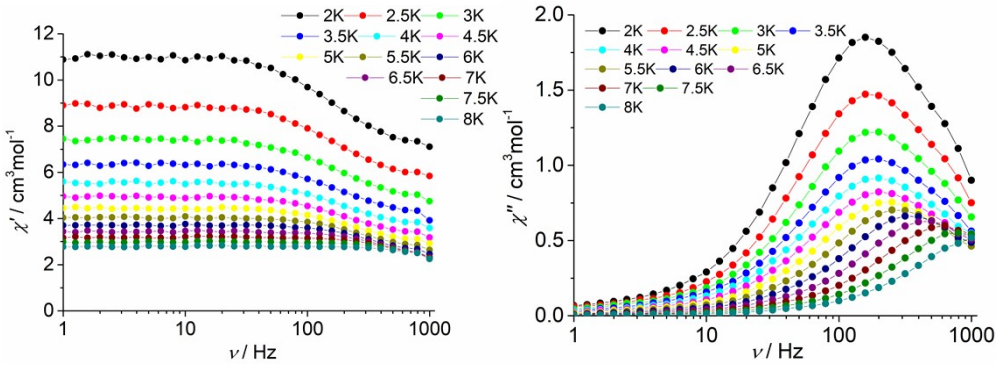

Fig. S11 The frequency dependent in-phase (χ') and out-of-phase (χ'') ac susceptibility under 0 Oe field for **3.**

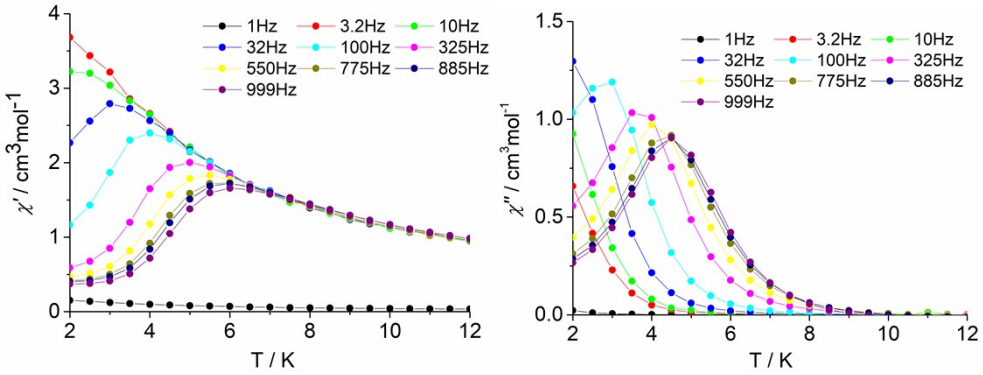

Fig. S12 The temperature dependent in-phase (χ') and out-of-phase (χ'') ac susceptibility under 800 Oe field for **1.**

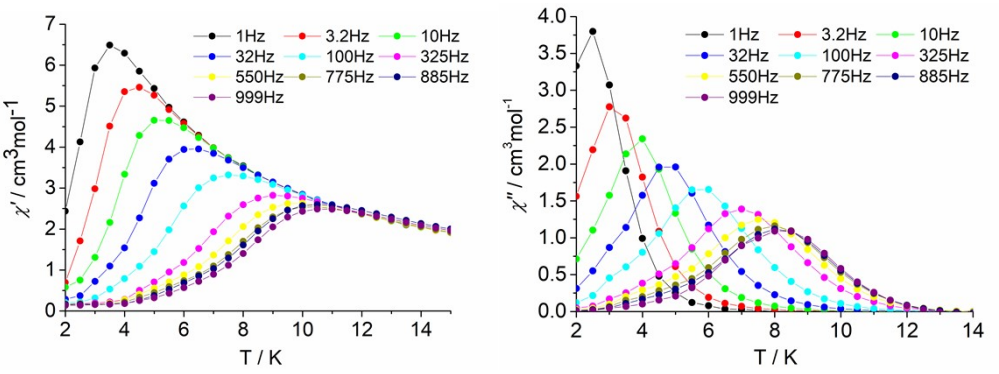

Fig. S13 The temperature dependent in-phase (χ') and out-of-phase (χ'') ac susceptibility under 1500 Oe field for **2.**

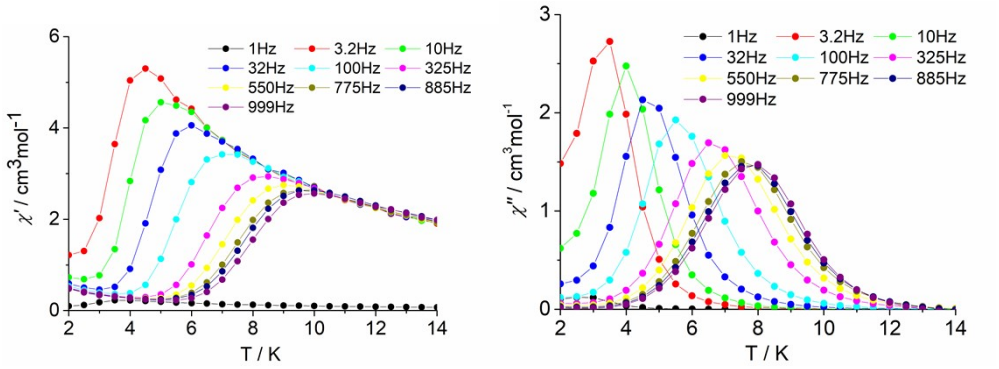

Fig. S14 The temperature dependent in-phase (χ') and out-of-phase (χ'') ac susceptibility under 1500 Oe field for **3.**

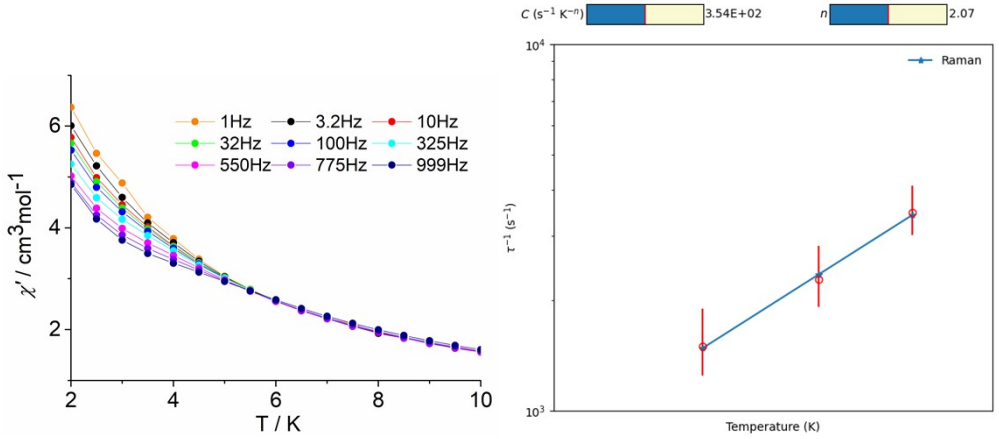

Fig. S15 The temperature dependent in-phase (χ') under 1500 Oe field for **4** (left) and the blue line represent the fitting of the frequency-dependent data by $\tau^{-1} = CT^{n}$ for **4** (right).

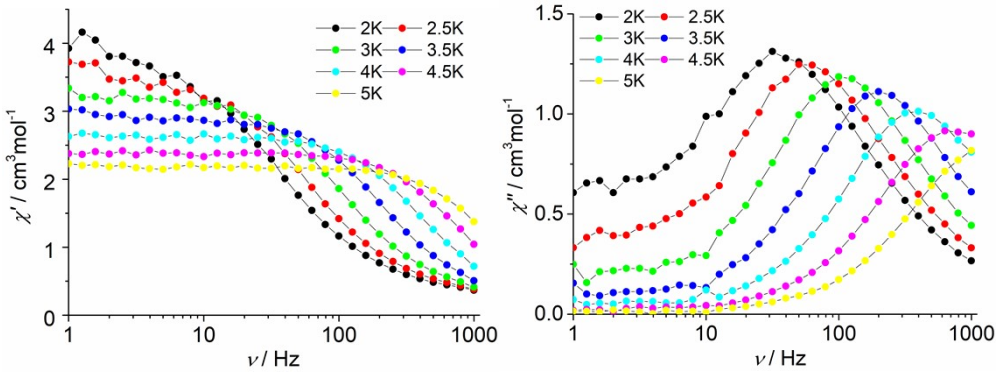

Fig. S16 The frequency dependent in-phase (χ') and out-of-phase (χ'') ac susceptibility under 800 Oe field for **1**.

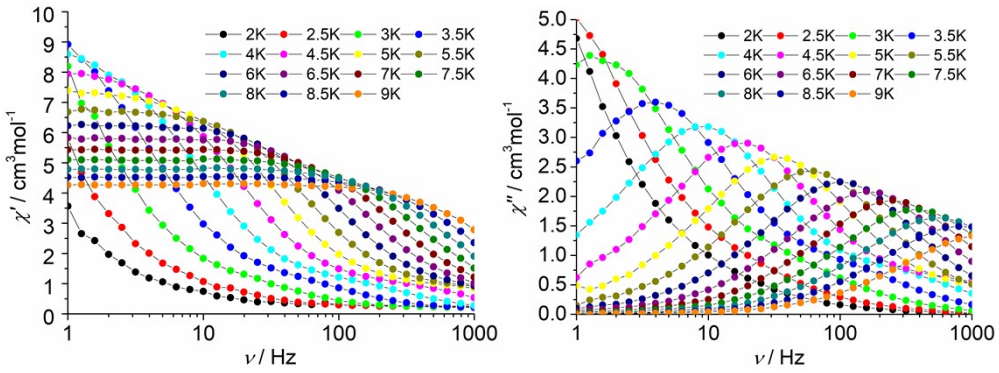

Fig. S17 The frequency dependent in-phase (χ') and out-of-phase (χ'') ac susceptibility under 1500 Oe field for **2**.

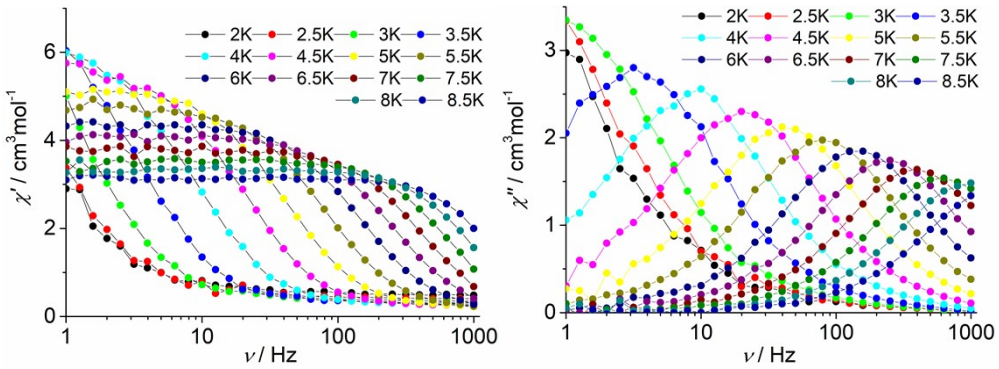

Fig. S18 The frequency dependent in-phase (χ') and out-of-phase (χ'') ac susceptibility under 1500 Oe field for **3.**

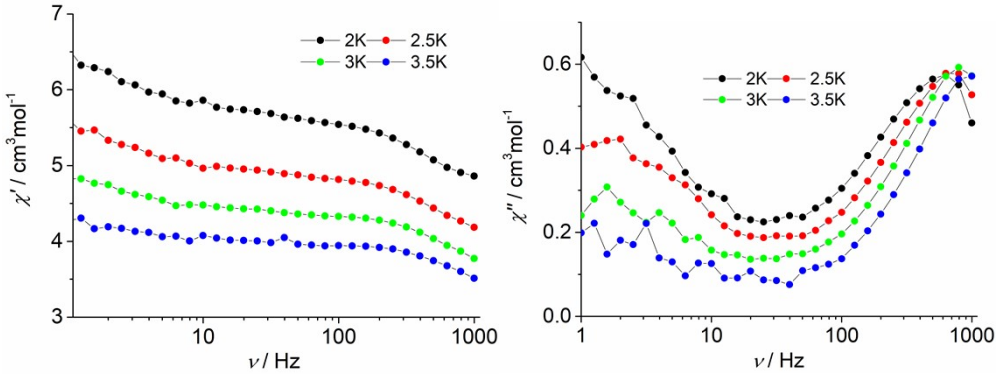

Fig. S19 The frequency dependent in-phase (χ') ac susceptibility and out-of-phase (χ'') ac susceptibility under 1500 Oe field for **4**.

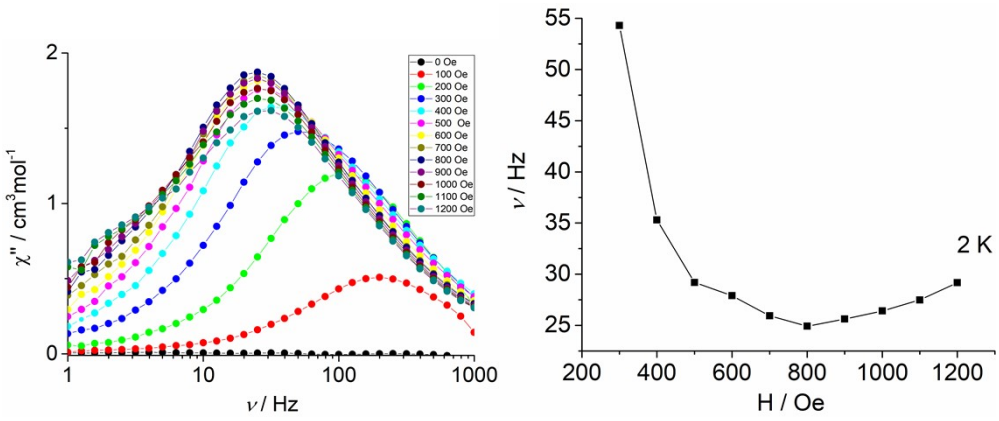

Fig. S20 The frequency dependence of the out-of-phase (χ'') ac susceptibility component at 2 K under different dc fields (left) and the frequency peak value of the dc external magnetic field at 2 K (right) for complex **1**.

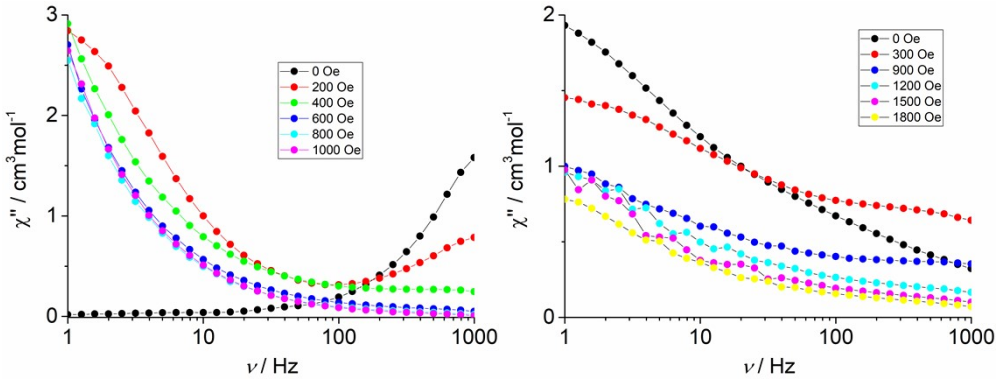

Fig. S21 The frequency dependence of the out-of-phase (χ'') ac susceptibility component at 2 K under different dc field for complexes **2** (left) and **3** (right).

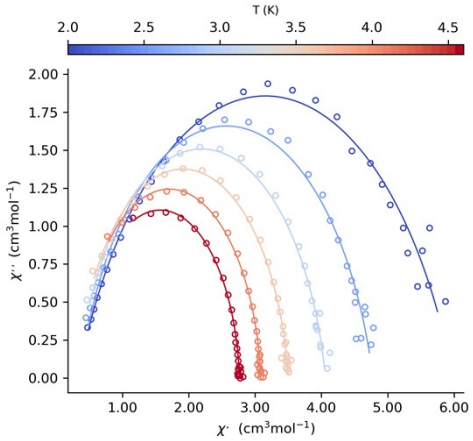

Fig. S22 Cole-Cole plots for the ac susceptibilities under 800 Oe dc field for **1**. The solid lines correspond to the best fit obtained with a generalized Debye model.

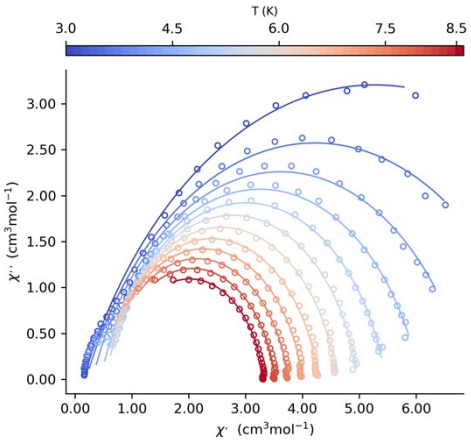

Fig. S23 Cole-Cole plots for the ac susceptibilities under 1500 Oe dc field for **2**. The solid lines correspond to the best fit obtained with a generalized Debye model.

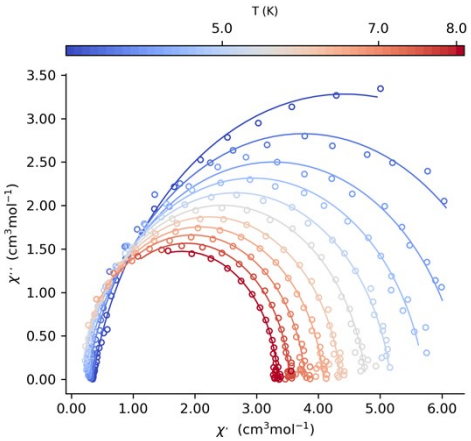

Fig. S24 Cole-Cole plots for the ac susceptibilities under 1500 Oe dc field for **3**. The solid lines correspond to the best fit obtained with a generalized Debye model.

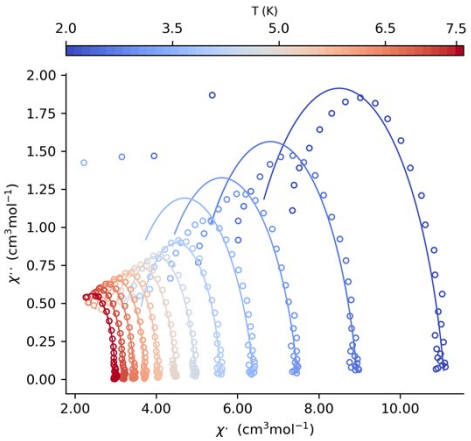

Fig. S25 Cole-Cole plots for the ac susceptibilities under 0 Oe dc field for **3**. The solid lines correspond to the best fit obtained with a generalized Debye model.

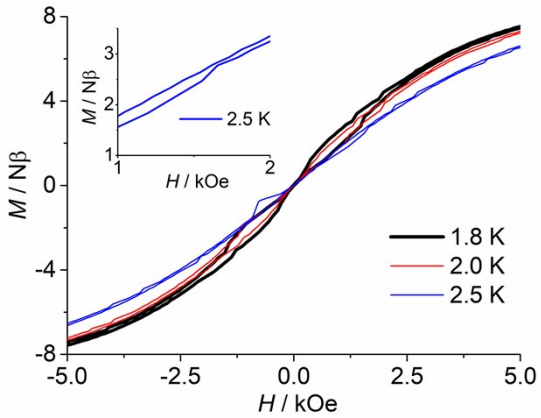

Fig. S26 Field dependence of the magnetization of **2** between 1.8 K, 2 K, and 2.5 K at a sweep rate of 200 Oe s^{-1}.

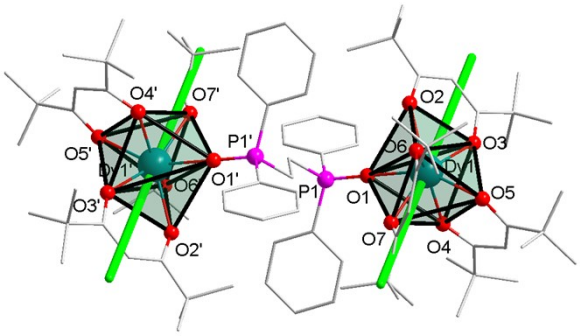

Fig. S27 Orientations of the anisotropy axes for each of the two Dy^{III} ions in **2** as calculated by MAGELLAN.

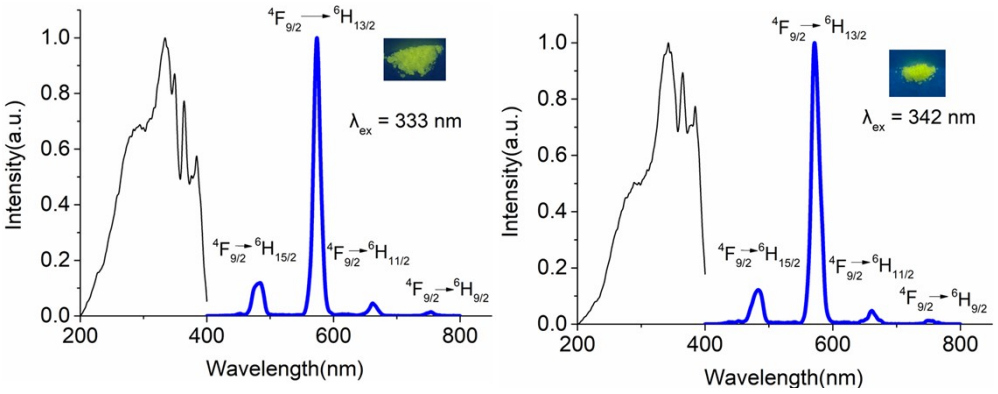

Fig. S28 Emission spectra of **1** (λ_{ex} = 333 nm) (left) and **2** (λ_{ex} = 342 nm) (right).

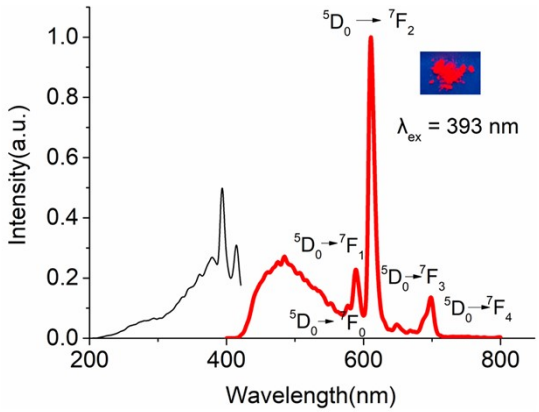

Fig. S29 Emission spectra of **5** (λ_{ex} = 393 nm).

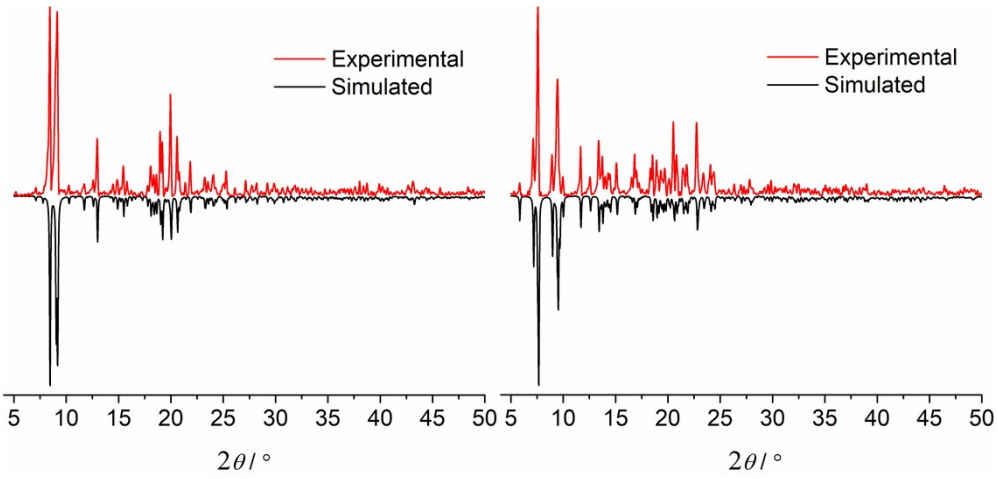

Fig. S30 Experimental and simulated powder X-ray diffraction (PXRD) patterns for **1** (left) and **2** (right).

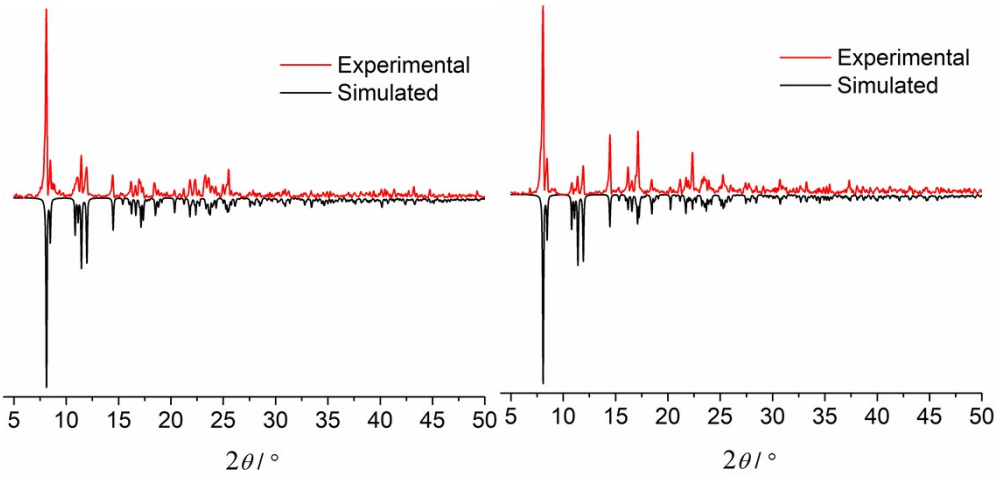

Fig. S31 Experimental and simulated powder X-ray diffraction (PXRD) patterns for **3** (left) and **4** (right).

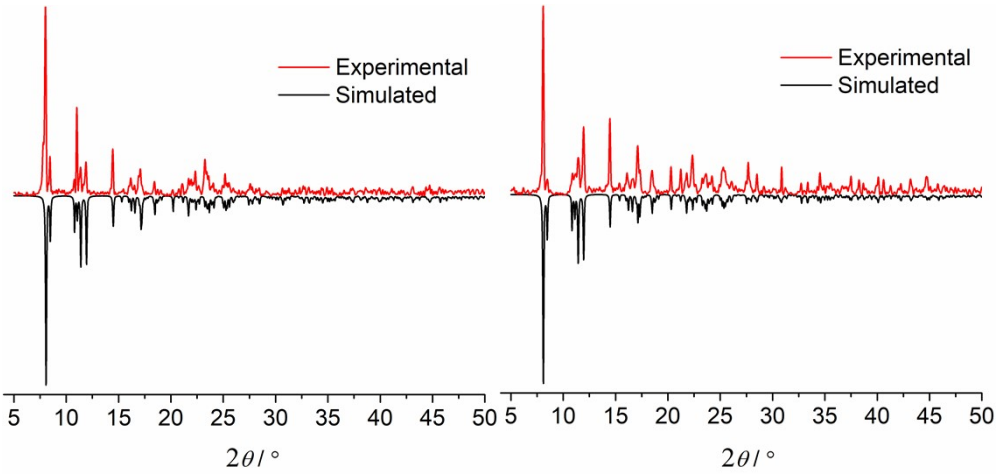

Fig. S32 Experimental and simulated powder X-ray diffraction (PXRD) patterns for **5** (left) and **6** (right).